Supporting information for: Seasonal dependence of geomagnetic active-time northern high-latitude upper thermospheric winds

Manbharat S. Dhadly[1], John T. Emmert[2], Douglas P. Drob[2], Mark G. Conde[3], Eelco Doornbos[4], Gordon G. Shepherd[5], Jonathan J. Makela[6], Qian Wu[7], Rick J. Niciejewski[8], and Aaron J. Ridley[8]

[1]National Research Council Postdoctoral Research Associate, Space Science Division, Naval Research Laboratory, Washington DC, USA

[2]Space Science Division, Naval Research Laboratory, Washington DC, USA

[3]Geophysical Institute, University of Alaska Fairbanks, Alaska, USA

[4]Aerospace Engineering, Delft University of Technology, The Netherlands

[5]Centre for Research in Earth and Space Science, York University, Canada

[6]Department of Electrical and Computer Engineering, University of Illinois at Urbana-Champaign, Illinois, USA

[7]High Altitude Observatory, UCAR, Colorado, USA

[8]Climate and Space Sciences and Engineering, University of Michigan, Ann Arbor, Michigan, USA

Contents of this file:

Text S1. GOCE Residual Winds

The data sets used in this research are obtained from multiple instruments operated independently of each other, with different technical implementations, modes of operations, and data processing algorithms. In our recent quiet-time study [*Dhadly et al.*, 2017], we compared various quiet-time data sets from the instruments used here and found no major biases (except some regional differences) among them except for GOCE. The GOCE cross-track winds as a function of magnetic latitude (MLAT) for various magnetic local time (MLT) bins were consistently different from the other data sets. The residual winds obtained from quiet-time GOCE and quiet-time wind climatology obtained from other data sets are shown in Figure S1. These results motivated us to statistically quantify the bias in GOCE cross-track winds as a function of MLAT. The details of empirically correcting the apparent bias in GOCE cross-track winds are presented in the main body (section 3) of this paper. The bias-corrected GOCE data are used for further analyses/comparisons.

Text S2. Magnetic Local Time Dependence

Using the coefficients of vector spherical harmonics (VSH) fits, we evaluate modeled wind fits at a MLAT-MLT regular grid and at the locations of the input observational data. To investigate the seasonal dependence of active-time high-latitude horizontal neutral winds as a function of magnetic local time, we first sorted modeled climatology and observational data into three seasonal bins (December solstice, equinox, and June Solstice). Further each seasonal bin data was divided into 5-degree MLAT and 1-hour MLT bins. The computed average zonal and meridional winds from each of these bins as a function of MLT are shown in Figure S2 and Figure S3, respectively. In these figures, the binned and averaged active-time winds obtained at MLAT-MLT regular grid are presented as "model cut" (black curve) and at the locations of observations are presented as "model average" (blue curve). The wind components are in magnetic coordinates. Any data point more than 3 standard deviations away from the initial fit was excluded from the analysis. The estimated uncertainty of the mean for each bin was calculated by dividing the standard deviation by the square root of the number of days in the sample as in *Emmert et al.* [2006, 2002]. For FPIs, we computed magnetic winds by averaging the observed geographic wind components and then projecting averaged wind vectors along magnetic directions. This is the same process as used in *Dhadly et al.* [2017]. The comparisons shown in these figures suggest no major biases among the various data sets (except some regional differences discussed in the main body of this paper). In this seasonal analysis, most of the daytime wind data is from WINDII green line measurements at 557.7 nm, and the major contributors on the nightside are SDIs and FPIs.

One of the main advantages of plotting winds a function of time is to check the consistency between daytime and nighttime data. As shows in Figures S2 and S3, the daytime winds are pretty consistent with the nighttime data with no significant discontinuity in winds (or big jumps in wind values). Overall, the active-time modeled winds show consistent progression from one bin to the next and empirical winds quantitatively and morphologically agree with observations with few minor discrepancies.

Differences between WINDII and other data sets are discussed in the main body of the paper (section 4). Another discrepancy exists between Alaskan SDIs (Poker Flat (PF) and Toolik Lake (TL)) and Sondrestrom (SS) FPI zonal winds (also seen in quiet-time seasonal climatology in *Dhadly et al.* [2017]). Alaskan SDIs are more than 100 ms^{-1} more eastward than SS FPI in equinox. This discrepancy could be due to the longitude dependence of high-latitude winds, given that Alaskan SDIs and Sondrestrom are widely separated in longitudes. Currently, the longitude dependence of high-latitude winds is not well understood. The zonal wind discrepancy between PF SDI and Millstone Hill (MH) FPI in 55–60 MLAT bin is most likely due to the difference in the latitudes of the observations within the latitude bin. The

PF SDI zonal winds in this bin are from the equatorward edge of its FOV ($\sim$60 MLAT) and MH FPI zonal wind are from the poleward edge of its FOV ($\sim$55 MLAT).

For Urbana (UR) and Peach Mountain (PM) FPIs, only measured line-of-sight (LOS) winds along geographic cardinal directions are reported in the available data. We used the given north-looking and south-looking LOS winds and calculated the north-looking and south-looking geographic meridional winds. Geographic zonal winds were calculated by averaging the east-looking and west-looking LOS winds. The calculated zonal and meridional winds as function of MLT are presented in Figure S4. Strong latitudinal gradients can exist in the meridional winds around mid-latitudes; therefore, to establish a comprehensive seasonal climatology of the active-time middle latitude winds, we have also included MH FPI winds in Figure S4. For a direct comparison between the model climatology and binned averages from these three middle latitude stations, first model climatology was binned and averaged in the same manner as observational data and then binned and averaged model winds were projected along the observational geographic cardinal directions. As shown in Figure S4, there is consistent progression of winds from one seasonal bin to the other, clearly illustrating the control of seasons on the winds. The strength of latitudinal gradients in meridional winds decreases with decreasing latitudes, but increases from winter to summer. With few discrepancies, overall the modeled wind morphology captures the salient features present in the observational data. On the average, in winter and equinox, the modeled meridional winds are more equatorward than observations below 51N MLAT, with an average difference of $\sim$25 ms^{-1}. All the three stations show a progressive shift in zonal wind from eastward to westward with the change in seasons: Zonal winds are more westward in summer than winter.

Text S3. Magnetic Latitude Dependence

To investigate the seasonal dependence of winds as a function of magnetic latitude, we first sorted modeled winds and observational data into three seasonal bins (December solstice, equinox, and June Solstice). Further each seasonal bin data were divided into 2-degree MLAT and 2-hour MLT bins. The computed average zonal and meridional winds from each of these bins as a function of MLAT are shown in Figure S5 and Figure S6, respectively. The quality control and error estimation procedures discussed in section S2 were used here. Figures S5 and S6 show overall good agreement between the binned averages of model and observational data. There is consistent progression of observed winds as function of magnetic latitude from one station to the other. Overall, the diverse data sets present a unified picture of the wind components. Modeled zonal and meridional wind climatology show similar wind morphology as the observational data except for a few discrepancies. The discrepancies between and WINDII and other data sets are discussed in the main body of the paper (section 4).

GOCE measurements (shown in Figure 1) are present on the dawnside and duskside in the form of a wide stripe covering middle to high latitudes. Its data overlap with multiple ground-based and space-based data sets. *Dhadly et al.* [2017] showed that GOCE was the probable cause of some discrepancies between model and other observations data. GOCE accelerometer (GOCE ACC) wind data consist of in situ cross-track winds (wind component perpendicular to the satellite track) derived using the measurements of on-board accelratometer, and hence cannot be directly compared with zonal and meridional wind components from other stations and model climatology. To establish a direct comparison between GOCE cross-track winds, other data sets, and model climatology, we used the method discussed in *Dhadly et al.* [2017] and calculated the cross-track winds for each station and model climatology by projecting their vector winds along the GOCE cross-track winds. The calculated cross-track winds as a function of MLAT and MLT are presented in Figures S7 and S8, respectively. The rightmost column in these figures illustrates the average unit vector along the GOCE cross-track with magnetic north being at the top of the page. Since GOCE was in near sun-synchronous dusk-dawn orbit, the average GOCE cross-track winds on the duskside and dawnside are essentially zonal; cross-track winds around noon are essentially meridional, as illustrated by GOCE unit vector. Due to such geometry, positive/negative cross-track winds on the duskside represents eastward/westward winds. The opposite is true on the dawnside.

References

Dhadly, M., J. Emmert, D. Drob, M. Conde, E. Doornbos, G. Shepherd, J. Makela, Q. Wu, R. Niciejewski, and A. Ridley (2017), Seasonal dependence of northern high-latitude upper thermospheric winds: A quiet time climatological study based on ground-based and space-based measurements, *J. Geophys. Res. Sp. Phys.*, *122*(2), 2619–2644, doi:10.1002/2016JA023688.

Emmert, J. T., B. G. Fejer, G. G. Shepherd, and B. H. Solheim (2002), Altitude dependence of middle and low-latitude daytime thermospheric disturbance winds measured by WINDII, *J. Geophys. Res. Sp. Phys.*, *107*(A12), SIA 19–1–SIA 19–15, doi:10.1029/2002JA009646.

Emmert, J. T., M. L. Faivre, G. Hernandez, M. J. Jarvis, J. W. Meriwether, R. J. Niciejewski, D. P. Sipler, and C. A. Tepley (2006), Climatologies of nighttime upper thermospheric winds measured by ground-based Fabry-Perot interferometers during geomagnetically quiet conditions: 1. Local time, latitudinal, seasonal, and solar cycle dependence, *J. Geophys. Res.*, *111*(A12), A12,302, doi:10.1029/2006JA011948.

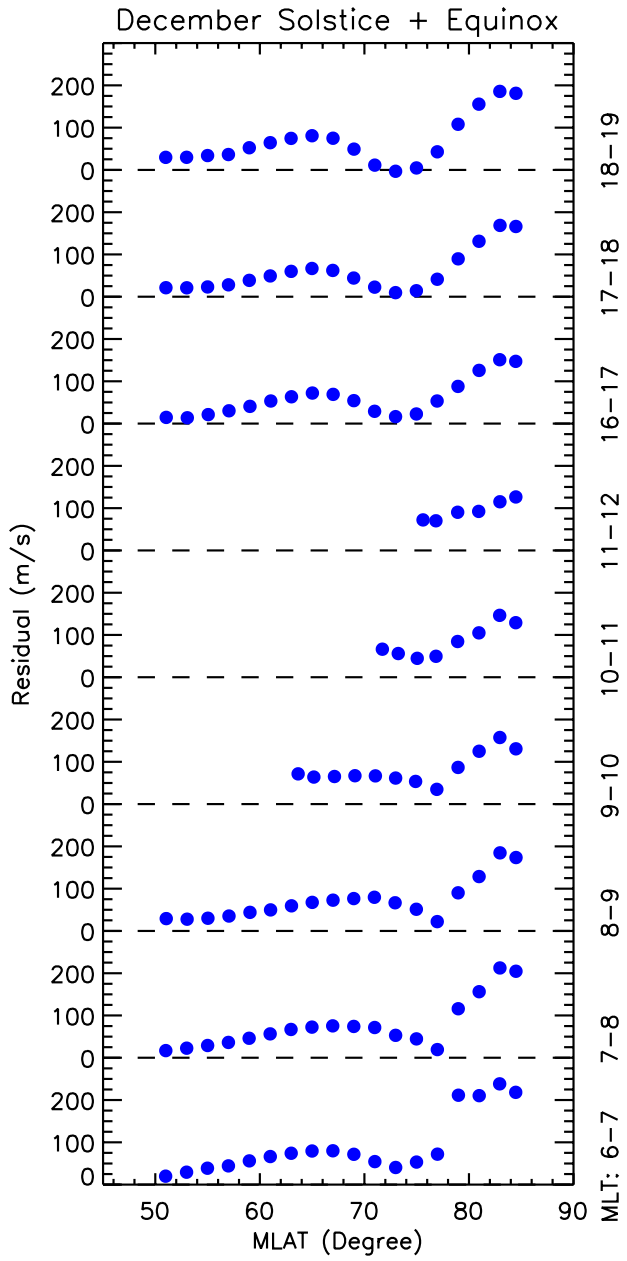

Figure S1. Residual winds (quiet-time GOCE cross-track – quiet-time modeled climatology without GOCE) as a function of magnetic latitude for various magnetic local time bins.

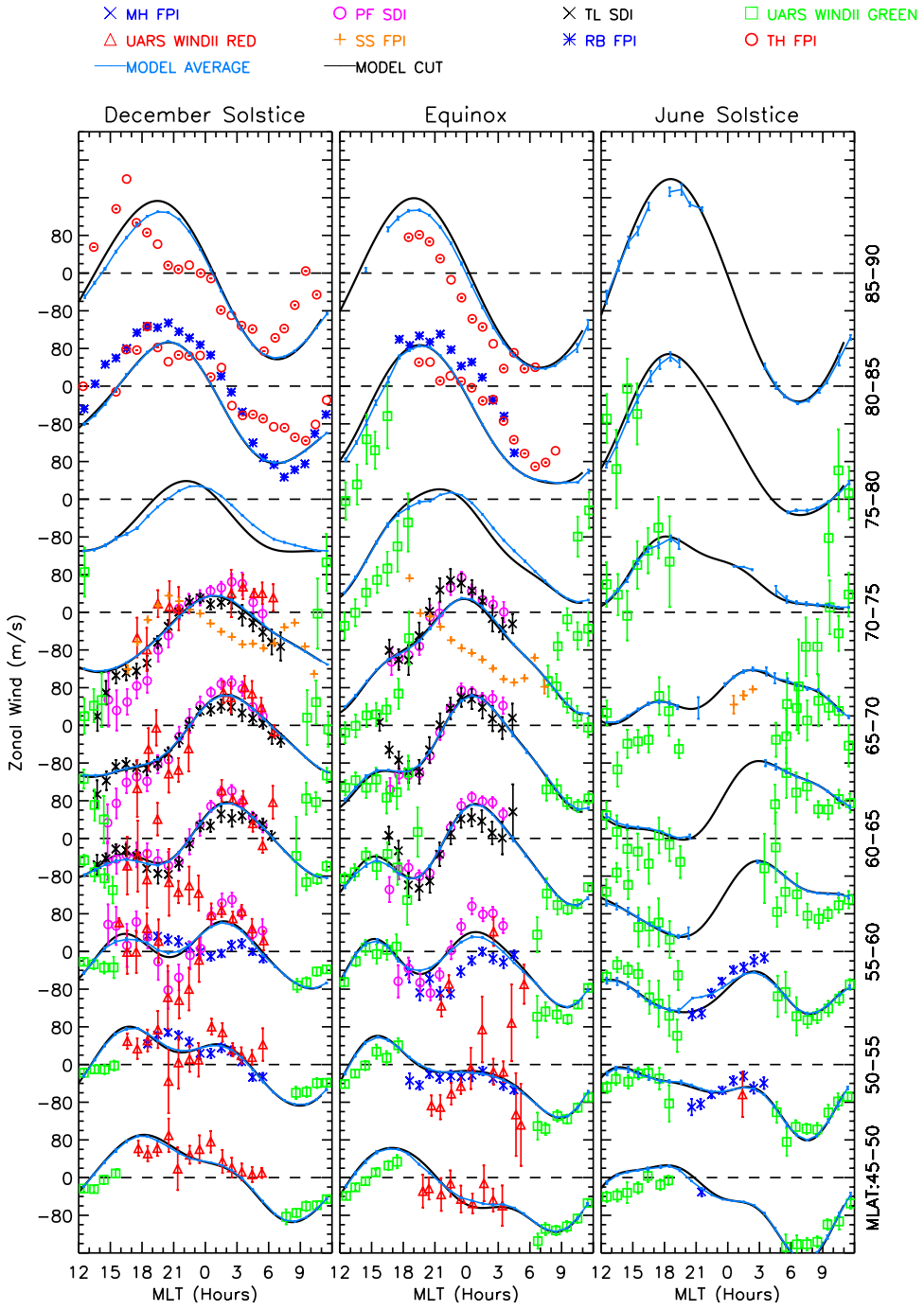

Figure S2. Comparison of active-time climatological zonal winds and observational data as a function of season and magnetic local time (hourly), for successive 5-degree magnetic latitude bins (annotated on right side y-axis). Observational data sets include data from ground-based FPIs (MH=Millstone Hill, SS=Sondrestom, RB=Resolute Bay, TH=Thule), SDIs (PF=Poker Flat, TL=Toolik Lake), and WINDII daytime and nighttime winds. Data stations are listed at the top of the figure. The blue curve shows average of model zonal winds at the locations of observations in each latitude bin. The black curve shows model zonal winds at the middle of each latitude bin. Error bars denote the estimated 1σ uncertainty of the mean (as in *Emmert et al.* [2006, 2002])

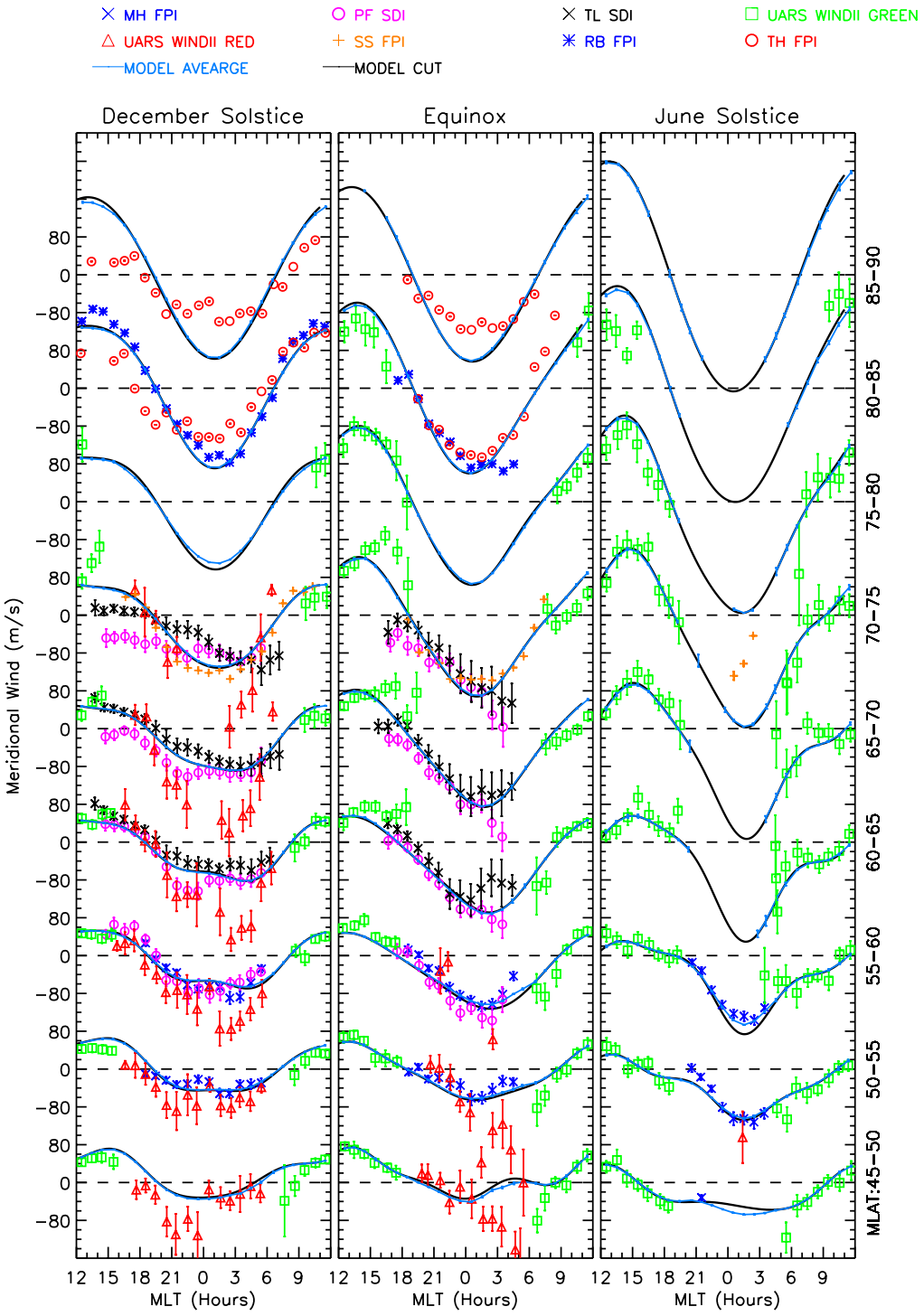

Figure S3. Same as Figure S2, but here showing meridional winds.

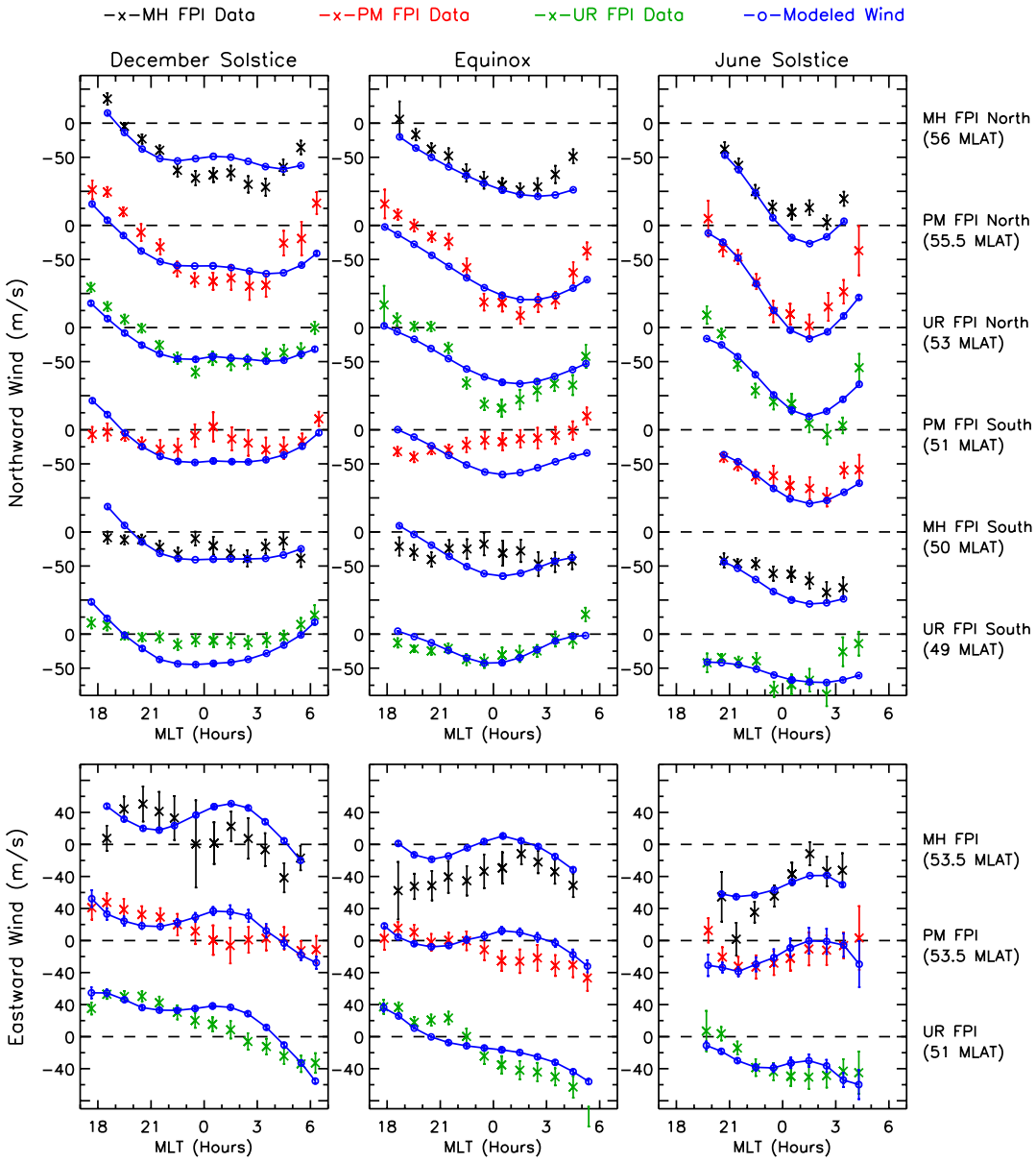

Figure S4. Comparison of active-time geographic northward (top) and eastward (bottom) winds from assimilated climatology with observational data from Millstone Hill (MH), Peach Mountain (PM), and Urbana (UR) FPIs for December solstice (left), equinox (middle), and June solstice (right). Average magnetic latitudes of the data are annotated on the right. Error bars indicate the estimated 1σ uncertainty of the mean.

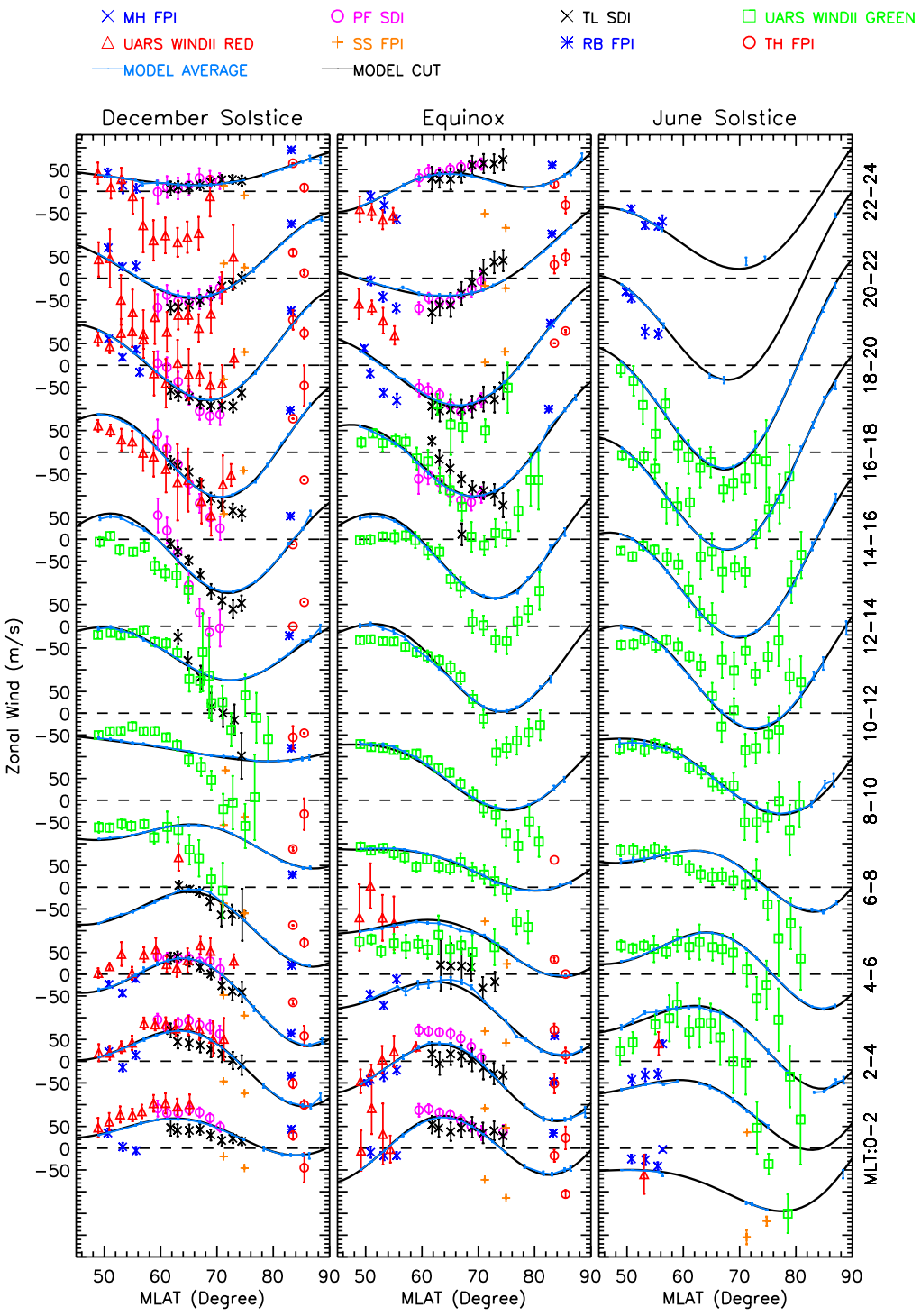

Figure S5. Same as Figure S2, but here showing data as a function magnetic latitude (2-degree bin), for successive 2-hour magnetic local time bins.

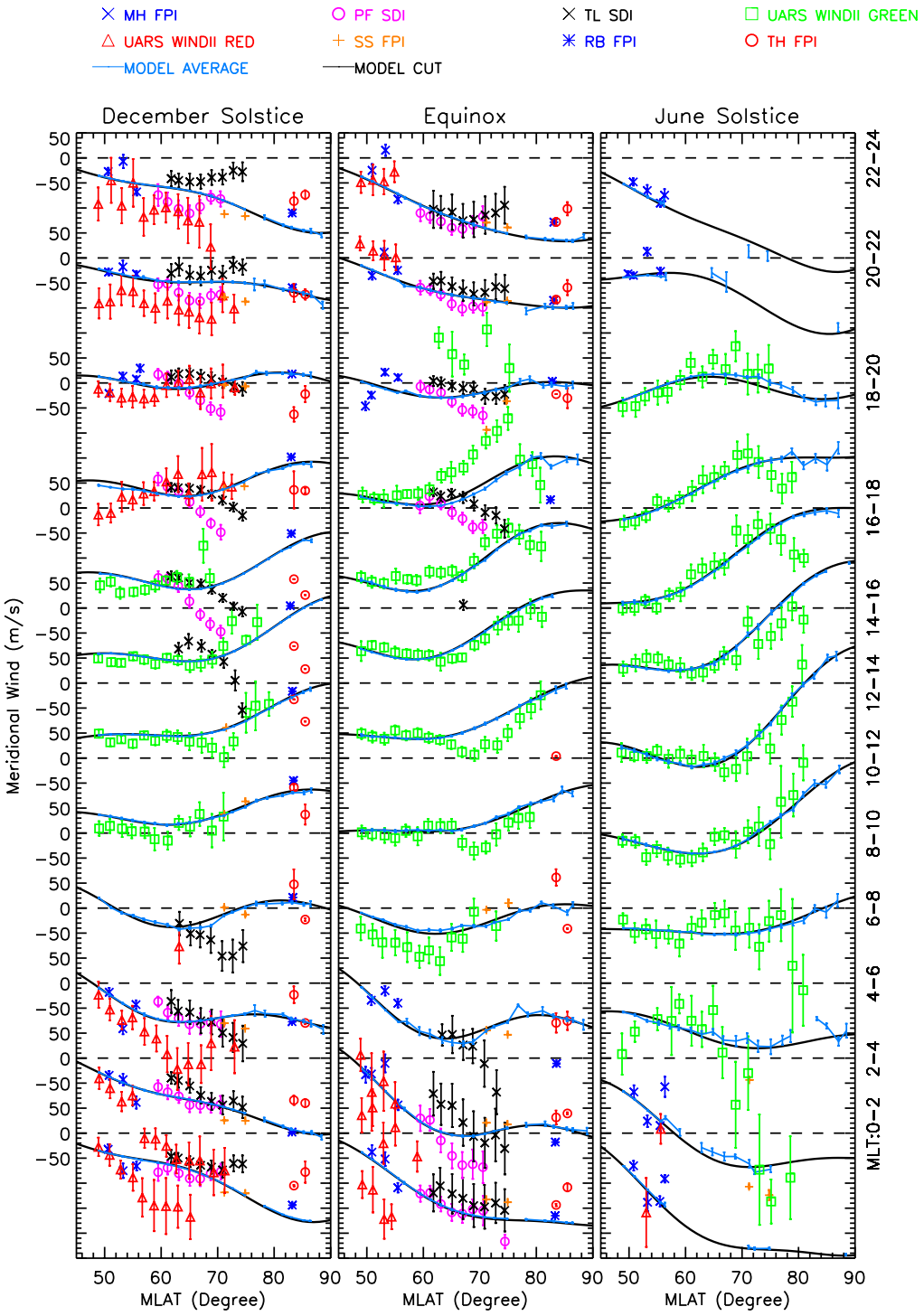

Figure S6. Same as Figure S5, but in this case showing meridional winds

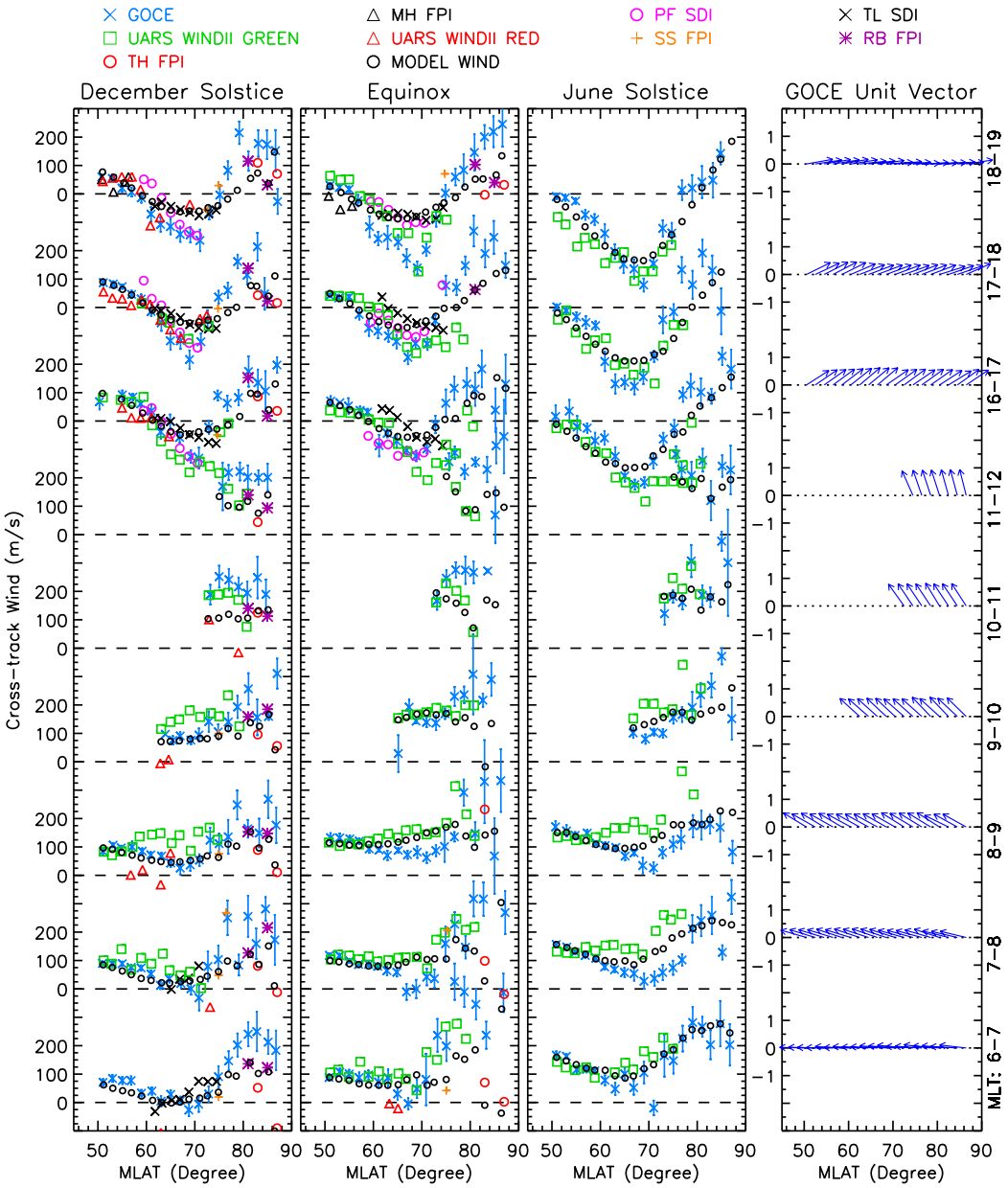

Figure S7. Comparison of active-time GOCE cross-track winds with the cross-track winds derived from modeled wind climatology, FPIs, SDIs, and WINDII data as a function of season and magnetic latitude (2-degree bin), for successive 1-hour magnetic local time bins around the dusk and dawn time sectors. The vectors in the rightmost column represent the average GOCE cross-track unit vector. For these unit vectors, magnetic north (east) is at the top (right) of the page.

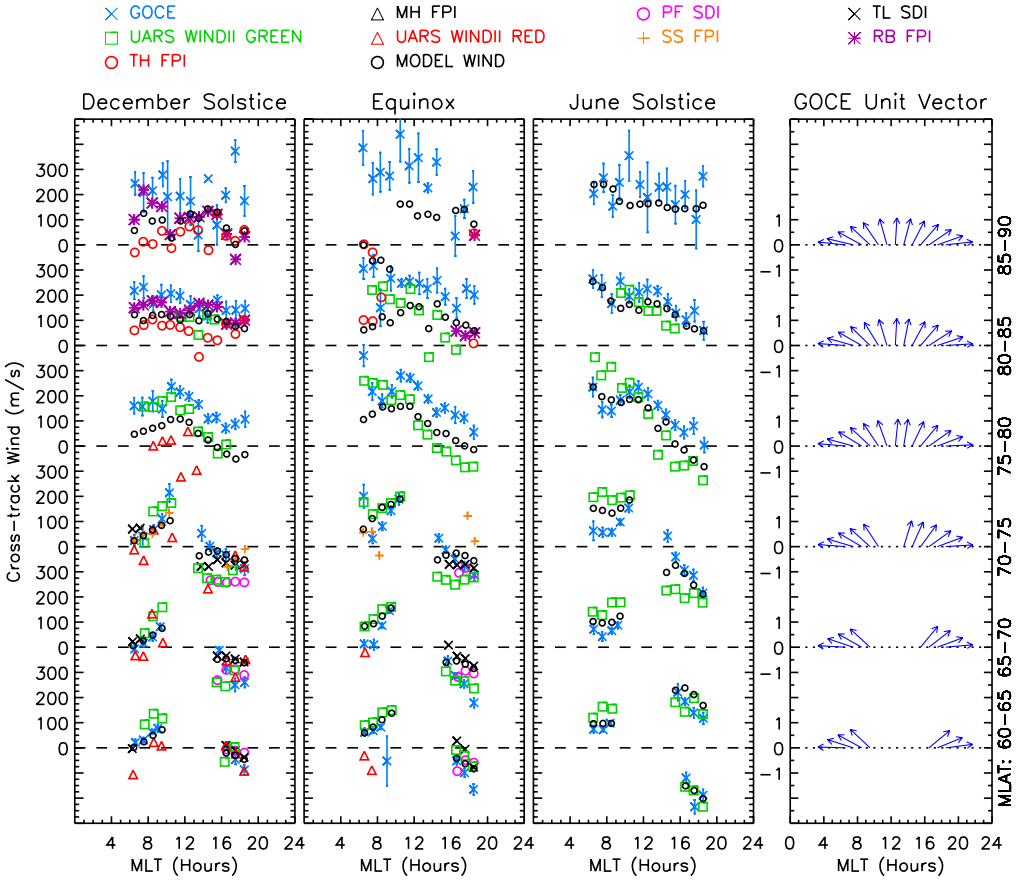

Figure S8. Same as Figure S7, but here showing cross-track winds as a function of magnetic local time (hourly), for successive 5-degree magnetic latitude bins above 60N.

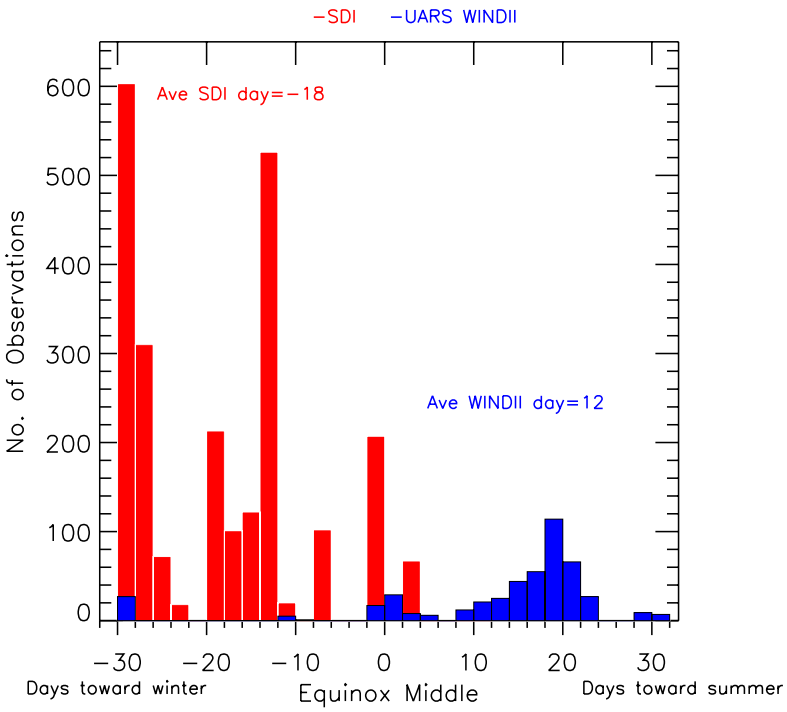

Figure S9. Data distribution of UARS WINDII green line and SDIs (PF SDI and TL SDI) in the equinox season between 60-75 MLAT in 16-18 MLT bin as a function of day. Red and blue colors represent SDI and WINDII green line data respectively. Zero on x-axis marks the middle of the equinox season. Negative/positive x-axis values are days from the middle of equinox towards the winter/summer season.

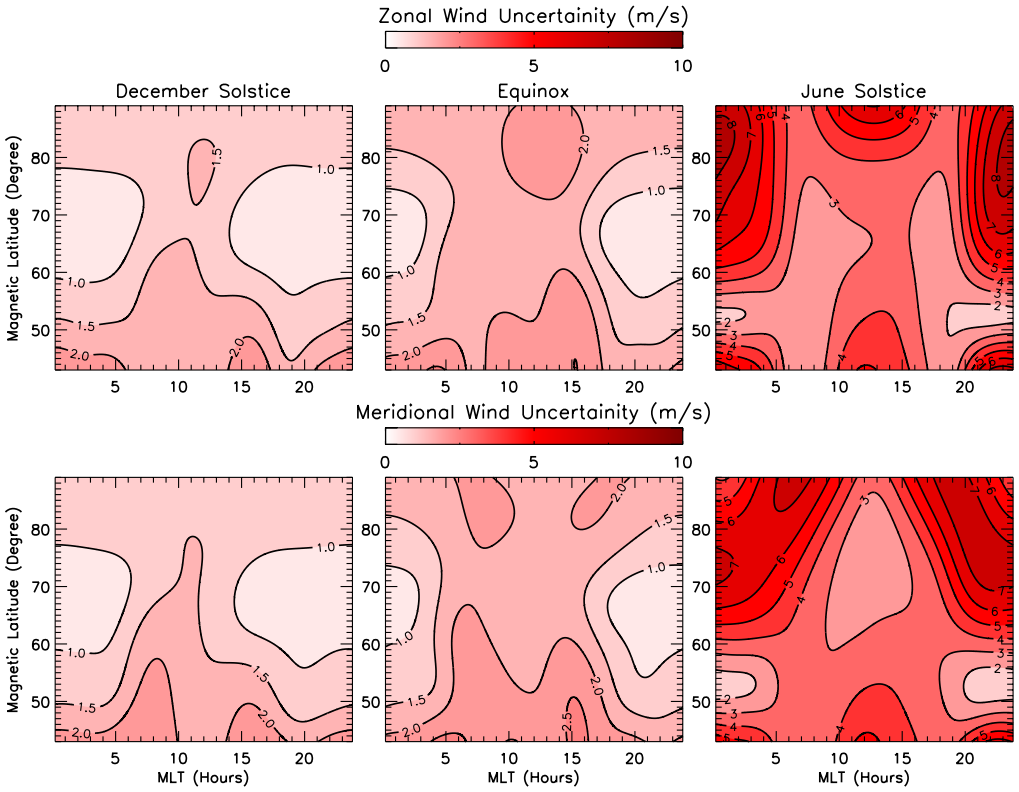

Figure S10. Estimated 1σ uncertainty in the modeled average zonal and meridional winds as a function of magnetic local time and magnetic latitude for December solstice (left column), Equinox (middle), and June solstice (right column).